MXene Anchored with TTPP-Stabilized Co Single Atoms for Accelerated Kinetics and Durable Li-Cl_2 Batteries

Xin-Ying Huang[a,†], Shang-Qi Li[b,†], Jiwei Liu[a], Xiao-Jie Yin[c,*], Chaofei Guo[a,*]

1. Experimental Section

1.1 *Materials:*

Propionic acid (AR, ≥ 99.5%), Pyrrole (99.0%), Cobaltous acetate tetrahydrate ($(CH_3COO)_2Co·4H_2O$, AR, ≥ 99.5%), Triethylamine (Et_3N, AR, ≥ 99.0%), N, N-Dimethylformamide (DMF, AR, ≥ 99.0%), Lithium chloride (LiCl, ≥ 97.0%), Lithium bis(trifluoromethanesulfonyl)imide (LiTFSI, ≥ 99.0%), Lithium Bis(fluorosulfonyl)imide (LiFSI, ≥ 98.0%), Thionyl chloride ($SOCl_2$, AR, ≥ 99.0%), Dichloromethane (CH_2Cl_2, ≥ 99.5%), Aluminum trichloride ($AlCl_3$, ≥ 99.0%) were bought from Sinopharm Chemical. 4-(4H-1,2,4-Triazol-4-yl)-Benzaldehyde (4T-BA), Mo_2TiAlC_2 powder were bought from Yanshen Technology Co., Ltd.

1.2 *Synthesis of 5 5,10,15,20-tetra(4-(1,2,4-trazol)-1-yl)phenyl)porphyrin (TTPP):*

Typically, 20 mL of propionic acid is added to a 100 mL three-necked flask, followed by 400 mg of 4-(4H-1,2,4-Triazol-4-yl)-Benzaldehyde (4T-BA). The mixture is stirred for 15 min to ensure complete dissolution. Then, 0.17 mL of pyrrole is slowly added dropwise to the mixture, and the reaction is carried out under reflux in the dark for 10 h. After the reaction is complete, the mixture is cooled to room temperature and allowed to stand overnight. The resulting product is collected by centrifugation, washed several times sequentially with acetone and deionized water, and finally dried under vacuum to yield the target crystalline product.

1.3 *Synthesis of Single-atom Co coordinated 5 5,10,15,20-tetra(4-(1,2,4-trazol)-1-yl)phenyl)porphyrin (SACo-TTPP):*

In a 50 mL glass vial, add $(CH_3COO)_2Co·4H_2O$ (125 mg), TTPP (50 mg), and triethylamine (Et_3N, 1.5 mL) into a mixed solvent consisting of methanol (MeOH, 10

mL), N, N-Dimethylformamide (1.2 mL) and sonicate until completely dissolved. Subsequently, the resulting solution was reacted at 100 °C for 24 h. After the reaction, the mixture was allowed to cool naturally to room temperature. The resulting deep brown powder was collected by centrifugation and washed several times with acetone. Finally, it was dried overnight under vacuum at 80 °C to yield the target product, SACo-TTPP.

1.4 *Synthesis of SACo-TTPP/$Mo_2TiC_2T_x$:*

A physically blended SACo-TTPP/$Mo_2TiC_2T_x$ sample was obtained by grinding SACo-TTPP and $Mo_2TiC_2T_x$ powders with a mass ratio of 1:1 for 30 mins.

1.5 *Synthesis of TTPP@$Mo_2TiC_2T_x$ and SACo-TTPP@$Mo_2TiC_2T_x$:*

1.0 g of Mo_2TiAlC_2 powder was slowly added to a concentrated hydrofluoric acid (HF) solution in a high-density polyethylene beaker, and the mixture was stirred continuously at 55 °C for 48 h. After the reaction, the mixture was centrifuged and washed repeatedly with distilled water degassed with argon until the pH of the supernatant reached 6-7. Subsequently, the resulting suspension was subjected to ultrasonic treatment for 3 h, and the product $Mo_2TiC_2T_x$ was collected. Next, 100 mg of $Mo_2TiC_2T_x$ was dispersed in an ethanol/water mixed solvent, and 200 mg of SACo-TTPP was added; the mixture was then subjected to ultrasonic treatment for 3 h to achieve thorough composite formation. Finally, the product was collected by centrifugation, washed several times with DMF, and dried in a vacuum oven for 8 h to obtain the final product, SACo-TTPP@$Mo_2TiC_2T_x$. TTPP@$Mo_2TiC_2T_x$ was synthesized using the same method, except that TTPP was used in place of SACo-TTPP.

1.6 *Materials characterizations:*

Scanning electron microscopy (SEM) images were acquired using a JSM-6700F microscope, and transmission electron microscopy (TEM) was conducted on Talos F200X G2, superX. X-ray diffraction (XRD) analysis was performed on a Bruker D8

ADVANCE diffractometer. X-ray photoelectron spectroscopy (XPS) was conducted on Kratos AXIS SUPRA spectrometer. The specific surface area and pore size distribution were determined using a Micromeritics ASAP 2460 analyzer. Fourier-transform infrared (FT-IR) spectra were recorded on a Nicolet iS50 spectrometer. Time-of-flight secondary ion mass spectrometry (TOF-SIMS) was performed on ION TOF-SIMS 5; High-angle annular dark-field scanning transmission electron microscopy (HAADF-STEM) was tested on Thermo Scientific spectra 300; Thermal Gravimetric (TG) was tested on HITACHI STA200/HITACHI STA300. Extended X-ray absorption fine structure (EXAFS) measurements was tested at Taiwan Light Source (TLS).

1.7 *Theoretical capacity calculated of the Li-Cl_2 battery:*

The theoretical capacity of the cathode was calculated to be 756 mAh g^{-1}, based on the formula: Q = nF/3.6M. n: the number of transferred electrons from one molecule, calculated to be 2, F: Faraday constant (96500 C mol^{-1}), M: molecular weight (70.9 g mol^{-1}) and Q: specific capacity (mAh g^{-1}).

1.8 *Electrochemical tests:*

The cathode electrode consisted of the active material, acetylene black and PVDF mixed in a mass ratio of 8:1:1, and was added to the NMP solvent. The slurry was then stirred for 30 min and dripped onto carbon paper. The mass loading of the active material in the electrode was about 1.2 mg cm^{-2}. The electrochemical properties of the working electrode were characterized in Swagelok cell, which was assembled in an Ar-filled glove box. Lithium foil was used as the counter electrode. GF/D was used as the separator. The electrolyte was prepared by dissolving 532 mg $AlCl_3$, 134 mg LiCl, 88 mg LiTFSI and 88 mg LiFSI in a mixture of 2 mL $SOCl_2$ and 2 mL CH_2Cl_2. The charge/discharge performance was examined on a LAND-CT2001 system. The charging process was capacity-limited (1000 - 4000 mAh g^{-1}), while the discharging process was terminated upon reaching a cutoff voltage of 2.0 V.

1.9 *Density Functional Theory (DFT) Calculations*

Spin-polarized density functional theory (DFT) calculations were performed using the generalized gradient approximation (GGA) with the Perdew-Burke-Ernzerhof (PBE) functional. The projected augmented wave (PAW) method and a plane-wave basis set with a cutoff energy of 500 eV were employed. Gaussian smearing with a width of 0.05 eV was used for partial occupancies. The convergence criteria were set to 10^{-5} eV for electronic self-consistency and 0.05 eV $Å^{-1}$ for geometry optimization.

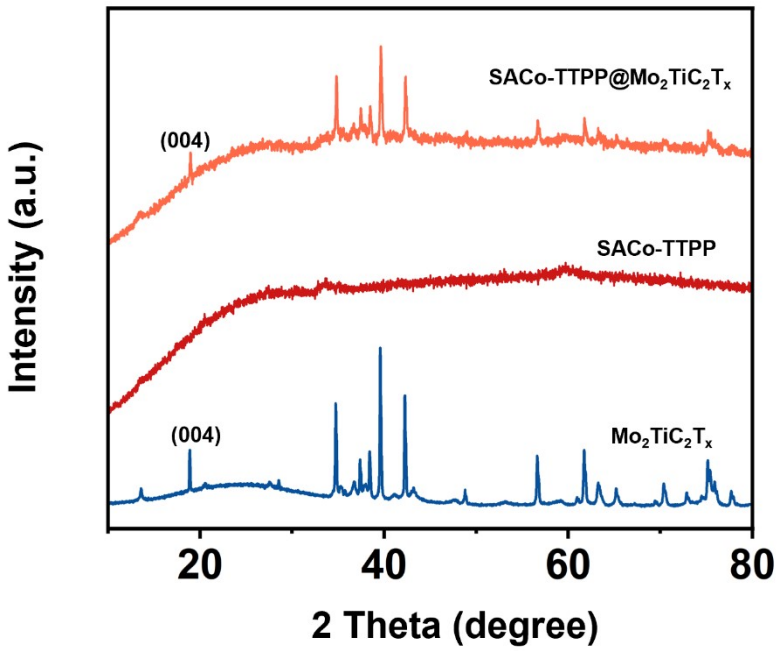

Figure S1 (a) XRD of the SACo-TTPP@$Mo_2TiC_2T_x$, SACo-TTPP and $Mo_2TiC_2T_x$.

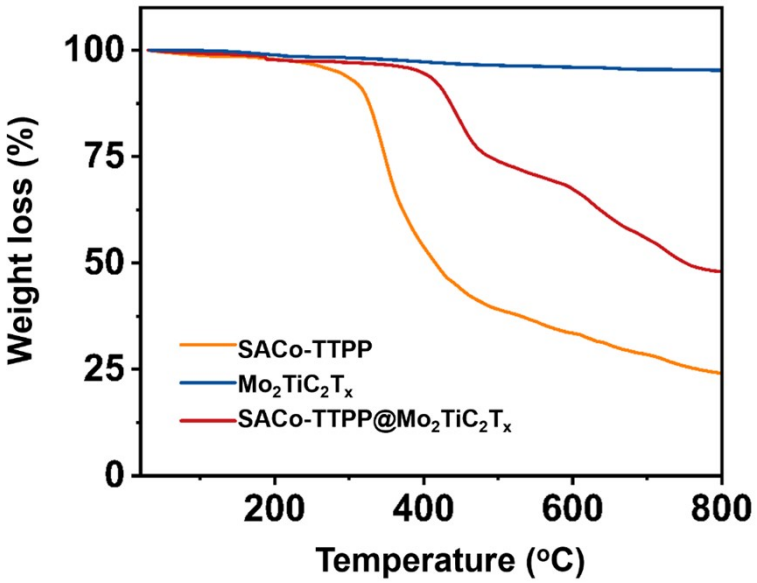

Figure S2 TG profiles under N_2.

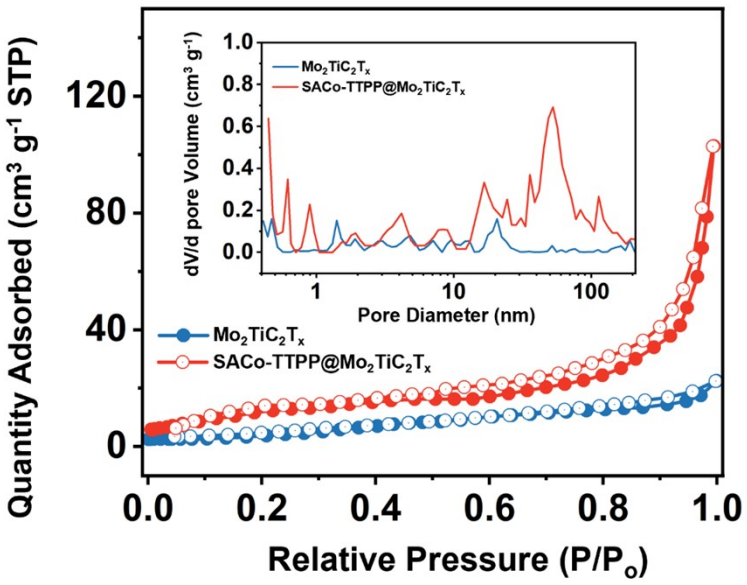

Figure S3 N_2 adsorption and desorption isotherms of SACo-TTPP@$Mo_2TiC_2T_x$ and $Mo_2TiC_2T_x$ at 77 K (insert: pore size distribution).

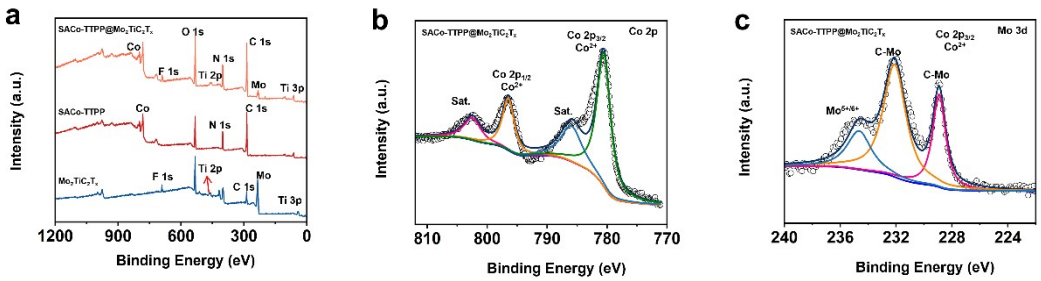

Figure S4 (a) The XPS profiles of SACo-TTPP@$Mo_2TiC_2T_x$, SACo-TTPP and $Mo_2TiC_2T_x$; (b) and (c) High resolution Co 2p and Mo 3d XPS spectra, respectively.

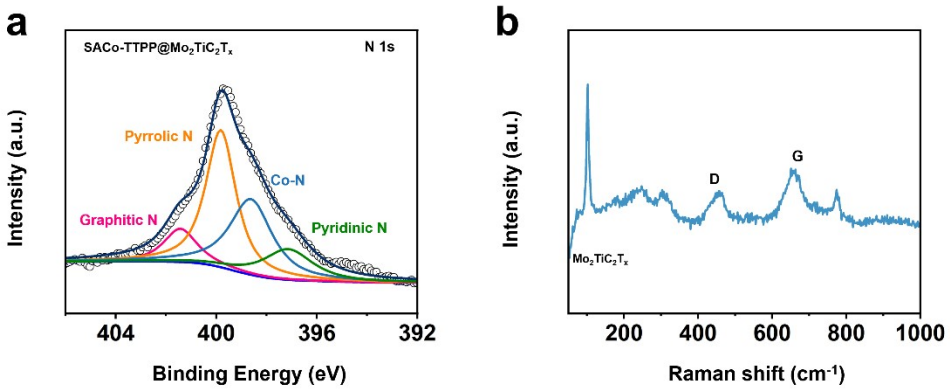

Figure S5 (a) High-resolution XPS spectra of N 1s for SACo-TTPP@$Mo_2TiC_2T_x$; (b) Raman spectra of $Mo_2TiC_2T_x$.

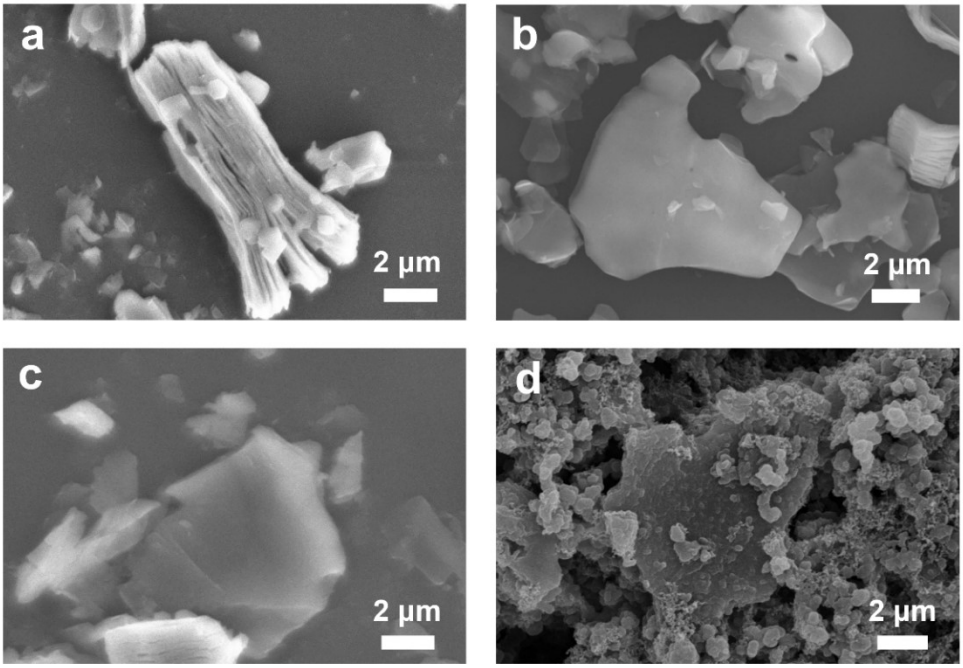

Figure S6 (a-c) SEM images of the $Mo_2TiC_2T_x$; (d) SEM images of the SACo-TTPP@$Mo_2TiC_2T_x$.

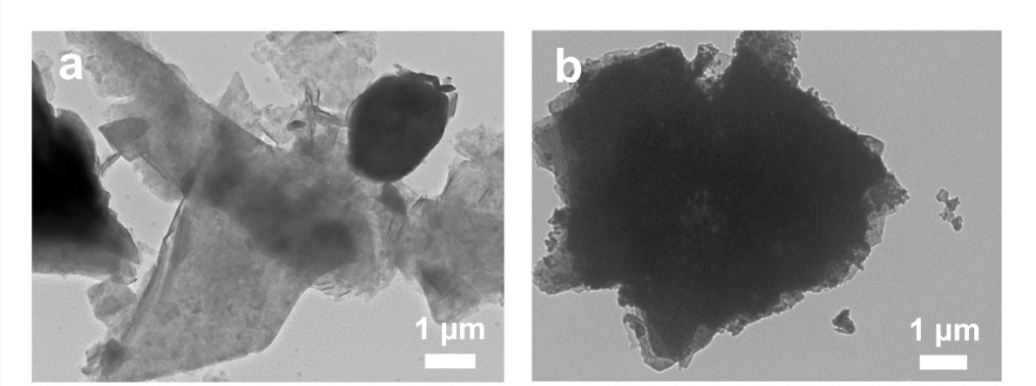

Figure S7 (a) TEM images of the $Mo_2TiC_2T_x$; (b) TEM images of the SACo-TTPP@$Mo_2TiC_2T_x$.

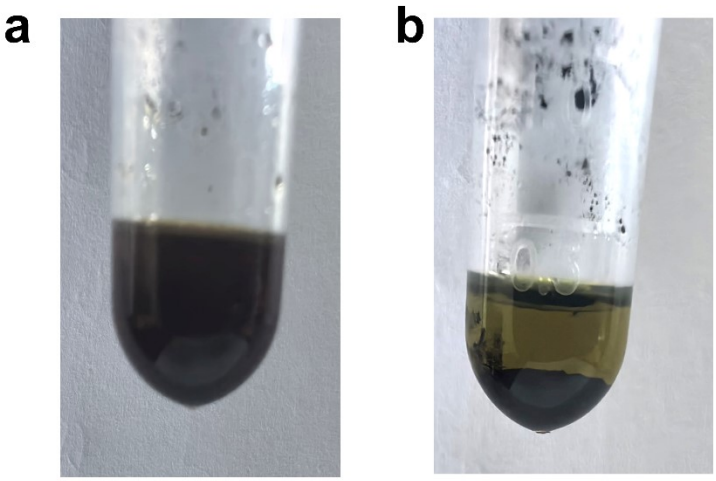

Figure S8 (a) Digital images of the solution of 6.0 mg SACo-TTPP dispersed in 0.5 mL $SOCl_2$-based electrolyte, (b) Solution of 12 mg SACo-TTPP@$Mo_2TiC_2T_x$ dispersed in 0.5 mL $SOCl_2$-based electrolyte.

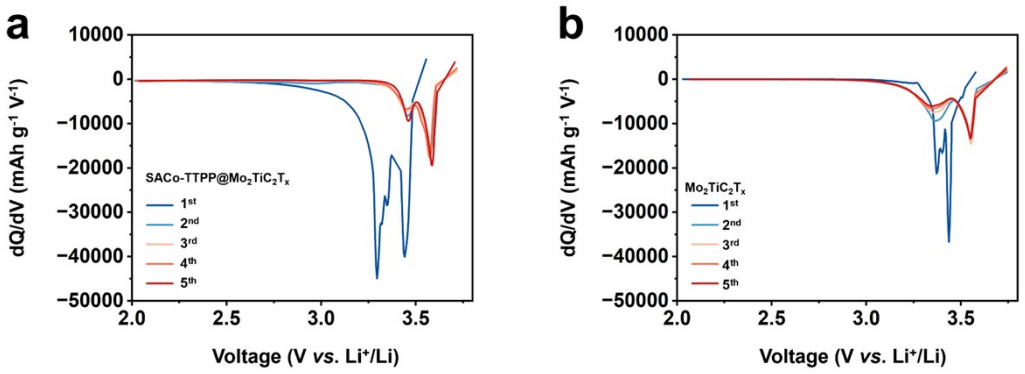

Figure S9 (a) dQ/dV curves of SACo-TTPP@$Mo_2TiC_2T_x$ electrode; (b) dQ/dV curves of SACo-TTPP@$Mo_2TiC_2T_x$ electrode.

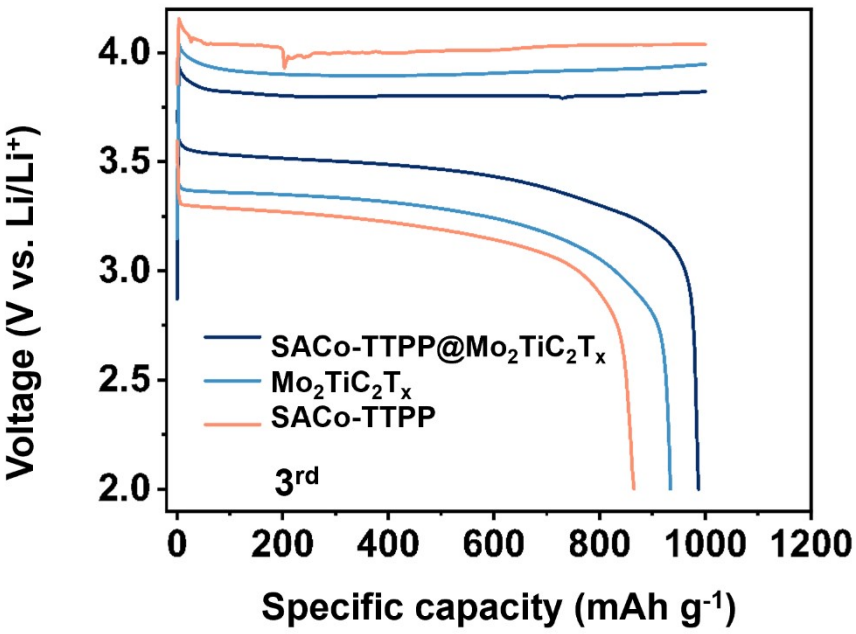

Figure S10 Discharge/charge curves of the SACo-TTPP@$Mo_2TiC_2T_x$, SACo-TTPP and $Mo_2TiC_2T_x$ electrode, respectively.

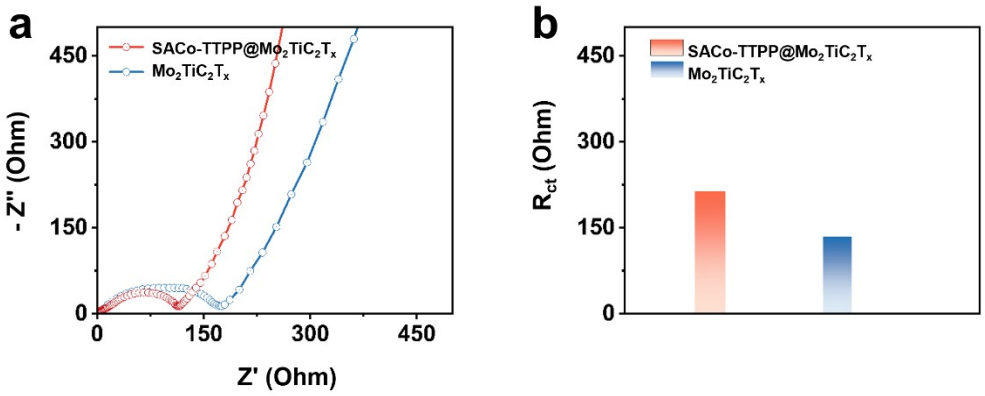

Figure S11 EIS Nyquist plots of (a) SACo-TTPP@$Mo_2TiC_2T_x$, and (b) $Mo_2TiC_2T_x$ electrodes upon discharging.

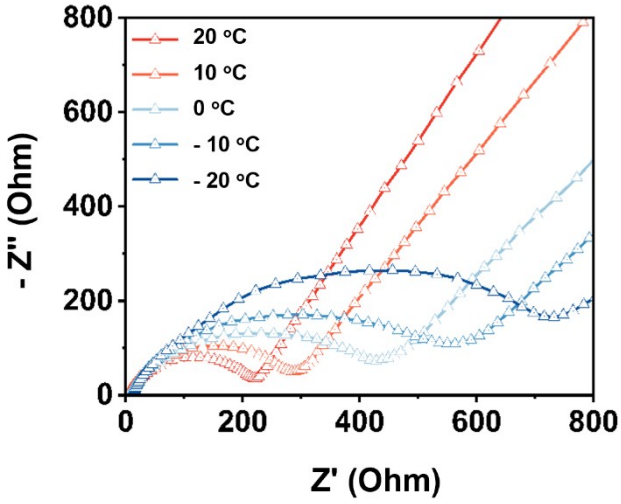

Figure S12 EIS Nyquist plots of $Mo_2TiC_2T_x$.

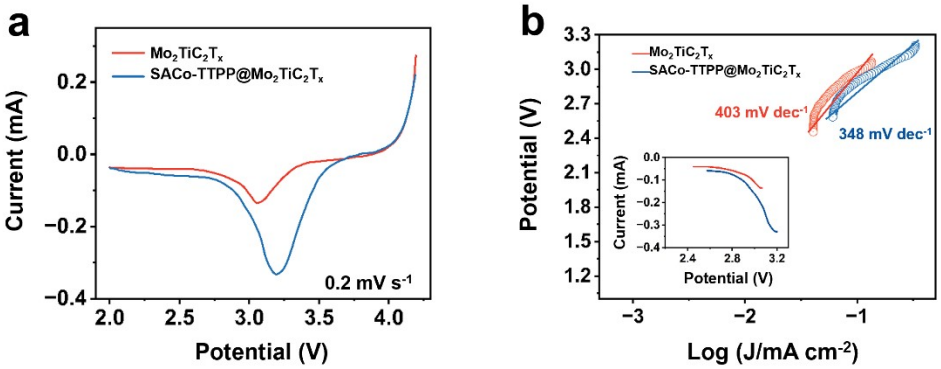

Figure S13 (a) CV curves of SACo-TTPP@$Mo_2TiC_2T_x$ and $Mo_2TiC_2T_x$ cathode; (b) Tafel plots derived from CV curves.

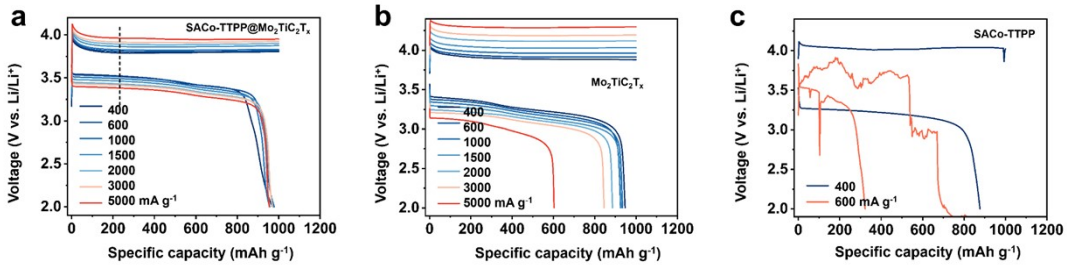

Figure S14 (a) Discharge/charge curves of the SACo-TTPP@$Mo_2TiC_2T_x$ electrode at various current density; (b) Discharge/charge curves of the $Mo_2TiC_2T_x$ electrode at various current density; (c) Discharge/charge curves of the SACo-TTPP electrode at various current density.

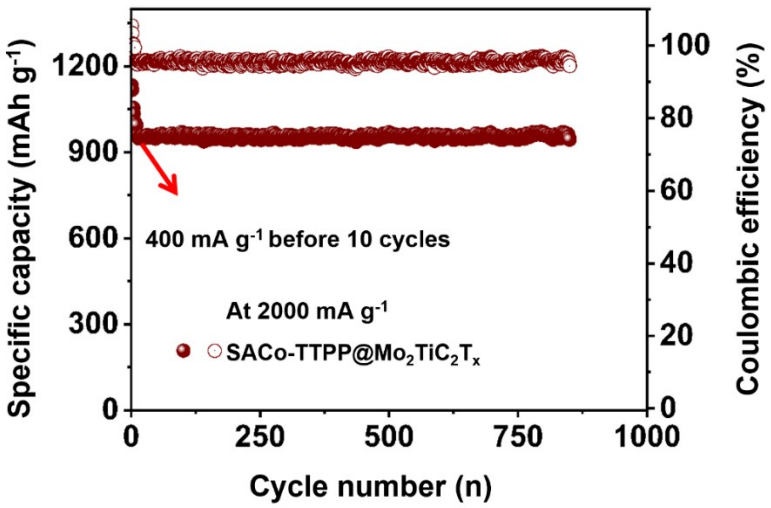

Figure S15 Cycling performance of SACo-TTPP@$Mo_2TiC_2T_x$ electrode at high current density of 2000 mA g^{-1}.

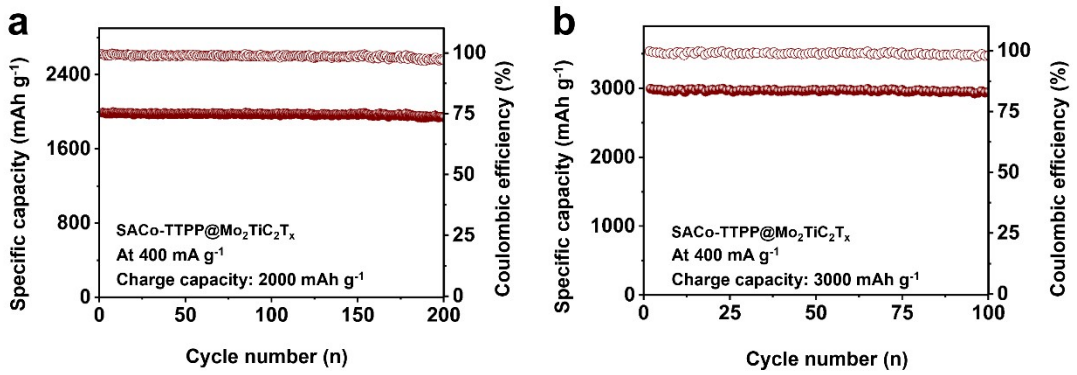

Figure S16 (a) Cycling performance of SACo-TTPP@$Mo_2TiC_2T_x$ electrode under charge capacities of 2000 and (b) 3000 mAh g^{-1} at 0.4 A g^{-1}.

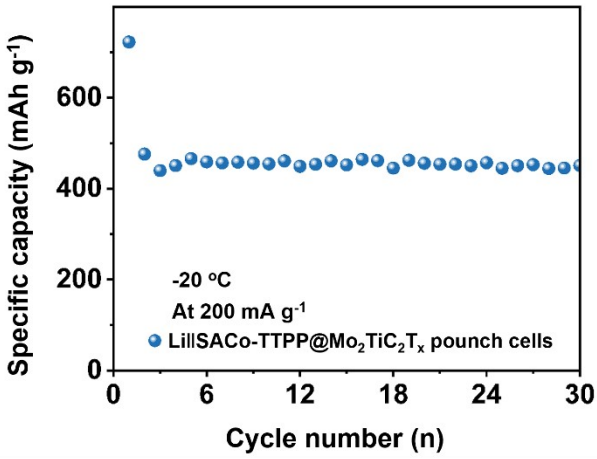

Figure S17 Cycling performance of pouch cells.

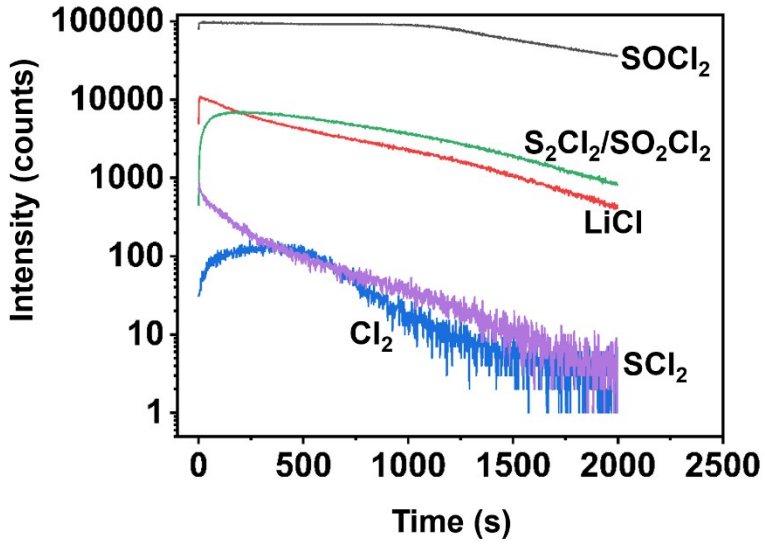

Figure S18 TOF-SIMS 3D distributions of different species at fully discharged SACo-TTPP@$Mo_2TiC_2T_x$ cathode.

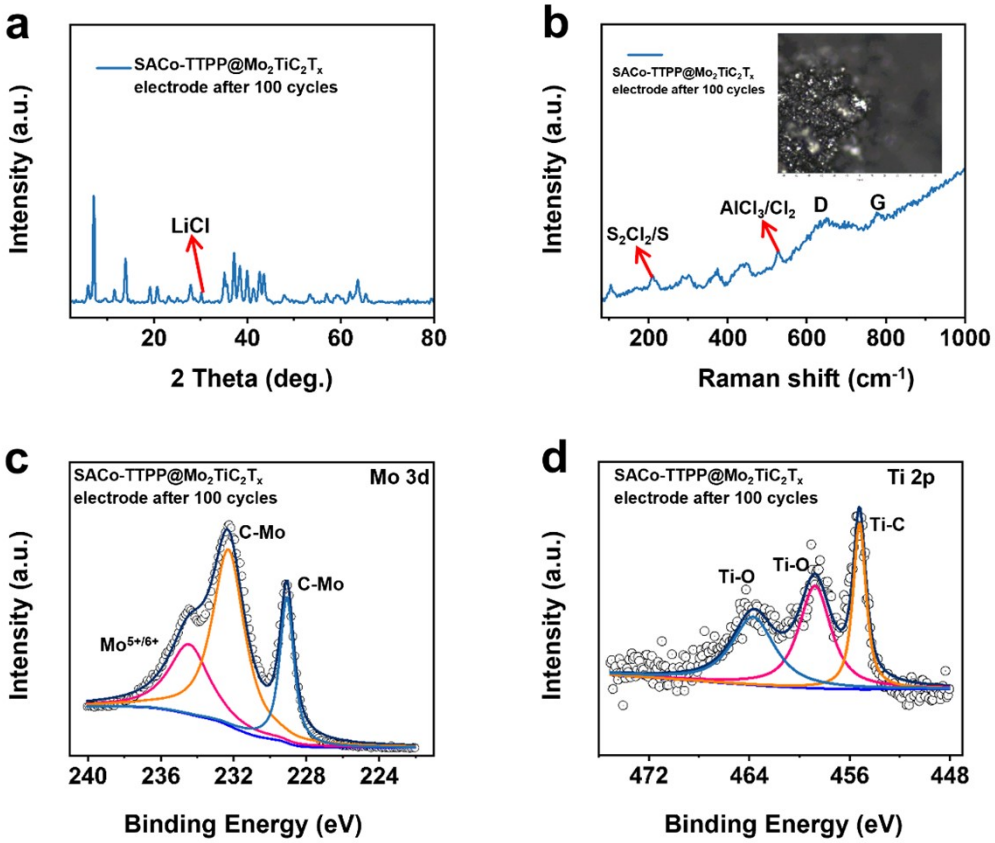

Figure S19 (a) XRD of SACo-TTPP@$Mo_2TiC_2T_x$ after cycles; (b) Raman of SACo-TTPP@$Mo_2TiC_2T_x$ after cycles; (c) Mo 3d XPS spectrum of SACo-TTPP@$Mo_2TiC_2T_x$ after cycles; (d) Ti 2p XPS spectrum of SACo-TTPP@$Mo_2TiC_2T_x$ after cycles.

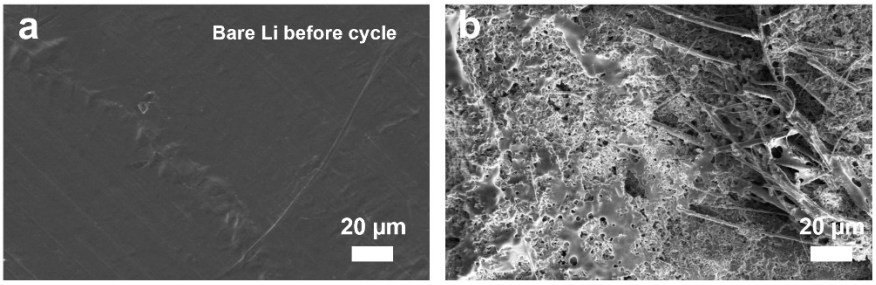

Figure S20 (a) SEM images of Li metal before cycle; (b) SEM images of Li metal with $Mo_2TiC_2T_x$ electrode after 100 cycles.

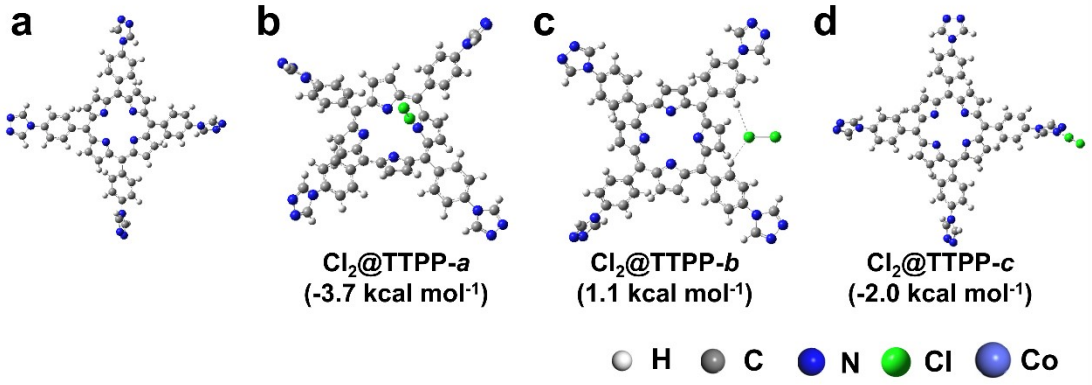

Figure S21 Molecular structure model of Cl_2 adsorbed on *a* site (a), *b* site (b), *c* site (c) in SACo-TTPP.

Table S1. Elemental analysis based on ICP-OES and CHNS measurements (wt.%).

Sample	C	N	H	Co	Mo	Ti	O	F
SACo-TTPP	60.11	28.85	4.29	6.75	\	\	\	\
$Mo_2TiC_2T_x$ MXene	8.05	0.2	0.2	\	69.64	16.20	3.91	1.8
SACo-TTPP@$Mo_2TiC_2T_x$	29.24	11.31	2.74	3.13	40.23	10.09	2.23	1.03

Table S2 *[a]CN* is the coordination number for the absorber-backscatter pair, *R* is the average absorber-backscatter distance, σ^2 is the Debye-Waller factor, and ΔE_0 is the inner potential correction. $*S_0^2$ was fixed to 0.79 as determined from Co foil fitting. The accuracies of the above parameters are estimated as *CN*, ±20%; *R*, ±1%; σ^2, ± 20%; ΔE_0, ±20%. The data range used for data fitting in k-space (Δk) and R-space (ΔR) are 3.0-11.0 $Å^{-1}$ and 1.0-2.0 Å, respectively. The XAFS data were processed using the ATHENA module implemented in the IFEFFIT software packages, and the least-square curve-fitting was accomplished by using the ARTEMIS module of IFEFFIT.

For Wavelet Transform analysis, the *χ(k)* exported from Athena was imported into the Igor Pro 6.10A. The parameters were listed as follow: *R*-range, 0-4.0 Å, *k*-range, 3.0-11.0 $Å^{-1}$ for sample and R-range, 0-4.0 Å, k-range, 3.0-12.0 $Å^{-1}$ for Standards; and Morlet function with κ=4, σ=2 was used as the mother wavelet to provide the overall distribution.

Sample	Path	*[a]CN*	*R*(Å)	$\sigma^2(10^{-3}Å^2)$	ΔE_0(eV)	R factor
Co foil	Co-Co	12	2.49±0.01	6.7±0.2	7.2±0.4	0.00095
SACo-TTPP@$Mo_2TiC_2T_x$	Co-N	4.4±0.4	1.95±0.01	8.0±1.2	-8.3±1.7	0.019

Table S3. Inductively coupled plasma (PerkinElmer ICP 2100) was used to characterize the mass content of Co in the sample. (m_0： quality of samples, g； V_0: volume of constant volume, mL; f: dilution factor; C_0: concentration of solution elements, mg L^{-1}; C_1: Elemental concentration of sample digestion solution raw solution, mg L^{-1}, C_1(mg L^{-1})=C_0(mg L^{-1})*f); C_x: Sample Elemental Content, mg kg^{-1}.

$C_x = \frac{C_0 * f * V_0 * 10^{-3}}{m * 10^{-3}} = \frac{C_1 * V_0 * 10^{-3}}{m * 10^{-3}}$, $Wt.(\%) = \frac{C_x}{10^6} * 100\%$.

Sample	Element	V_0	C_0	f	C_1	C_x	Wt. (%)
SACo-TTPP@$Mo_2TiC_2T_x$	Co	50	3.1742	10	31.7420	31556.3	3.15